Dalton Transactions

Accepted Manuscript

ROYAL SOCIETY OF CHEMISTRY

www.rsc.org/dalton

New insights into the nitroaromatics-detection mechanism of the luminescent metal-organic framework sensor

Lei Liu,[ab] Xiaofang Chen,[b] Jieshan Qiu[a] and Ce Hao*[a]

ABSTRACT: Luminescent metal-organic frameworks (LMOFs) have emerged as a group of new and very promising optic sensors in the detection of explosives. However, fundamental understanding of the sensing mechanisms on these materials is still immature and detailed investigations are needed. In this contribution, density functional theory (DFT) and time-dependent density functional theory (TD-DFT) are applied to reveal the underlying principles for the sensing mechanism by comprehensively studying the analyte-sensor interactions. Three molecules namely nitrobenzene, benzene and acetone are chosen as analytes while a newly reported explosives-detecting LMOF $[Zn_2(L)(bipy)(H_2O)_2]\bullet(H_2O)_3(DMF)_2$ is chosen as the sensor. Roles of two fundamental weak interactions namely hydrogen bonding interaction and π–π stacking interaction are clarified for the first time. By studying both the periodic crystal models and cluster models we obtain an in-depth understanding of the detecting mechanism from the view of electronic coupling. We find that intermolecular electron transfer is the inducement for the luminescence quenching detection of explosives. A brand new pathway for this electron transfer process is proposed for the first time. Most significantly, we discover that hydrogen bond shows multi-functions during the detecting processes which, on one hand, serves as the electron transfer bridge, on the other, reinforces the π–π stacking. This cooperative effect of the two weak forces inside MOFs is investigated for the first time, which not only provides valuable insights into the understanding of the analyte-sensor interactions inside the sensors but also offers useful guidance in the design of MOFs sensors to achieve high sensitivity.

Introduction

Increasing terror attacks using nitroaromatic compounds have claimed countless casualties and economic losses leaving poor and panic-stricken people. Thus, precise detections of these life-threatening explosive molecules play significant roles in anti-terrorism and civil security. Diverse detection methods from traditional sniffer dogs to state-of-art analytical instruments[1-4] have emerged and showed good performances in probing explosives. However, most of these methods suffer major drawbacks such as high costs and poor portability which prevent them from widespread applications. Optical detection is a promising method which has emerged and gained growing attentions in recent decades. Organic conjugate polymers[5-8] have been widely used in building this kind of optical sensors which have gained reputations as cheap, fast and portable. Since then, many new materials have been synthesized to achieve faster, more specific and more sensitive explosives detections.

Luminescent metal-organic frameworks (LMOFs) have emerged as a new group of promising optic detecting candidates for their unique structural and optical properties.[9-15] When interacting with explosives, LMOFs can encapsulate the analytes and exhibit luminescence quenching[16-25] or spectrum shifting.[26-28] Their porosity and luminescent properties can be finely tuned by using different metals and organic ligands in order to achieve specific detections. By tuning the size and chemical environment of the pore, a delicately designed LMOF can primarily eliminate the relative bulky interferential molecules, preconcentrate the analyte, increase the chance of guest-host interaction and efficiently recognize the explosive molecule. The diversity of metal (or metal cluster) centers and organic ligands makes it possible to design numerous LMOFs for detection purposes, which is an apparent advantage for MOF based sensors. However, this kind of diversity also makes it hard for one to select the proper building blocks from the vast ocean of candidates to achieve specific analyte detection. Thus, a clear understanding of the detecting mechanism of LMOFs should be the precondition and transplantable rules are needed to govern the selection of those building blocks.

LMOF $[Zn_2(L)(bipy)(H_2O)_2]\bullet(H_2O)_3(DMF)_2$ (1) (H_4L=bis-(3,5-dicarboxy-phenyl)terephthalamide, Figure S1, Supporting Information) is a typical explosives detecting candidate which was first synthesized in 2013 by Wang and co-workers (detailed structural information in reference 22). The strong emission of 1 was remarkably quenched by nitroaromatics (as much as 90%) while unaffected by alcohols, ketones, chloroalkanes and even other aromatic compounds. Up to now, this kind of promising explosive-detecting LMOFs via luminescence quenching phenomenon is quite common and syntheses of several similar functional LMOFs have been reported.[16-28] Considering the electron withdrawing ability of nitroaromatics, this kind of luminescence quenching mechanism has been generally attributed to the photo induced intermolecular electron transfer from the valence band (VB) of LMOF to the conduction band (CB) of LMOF then to the LUMO of the electron-deficient analyte.[16-19,29] Indeed, the flow of electrons from the electron-rich LMOF to the electron-deficient explosives can lead to luminescence quenching of the sensor. However, there should be some other pathways for the intermolecular electron transfer except for the aforementioned VB→CB→LUMO pathway. This issue, as far as we know, has never been concerned.

More important, intermolecular electron transfer process is closely related to the analyte-sensor interaction. Without considerable intermolecular interaction, electron transfer is not likely to occur even in the presence of proper driving force.[16] Hydrogen bonding interaction and π-π stacking interaction are common intermolecular interactions which can tune the optical properties of small organic dyes as well as metal-organic clusters.[30-32] In the case of LMOFs interacting with nitroaromatics, these two weak forces usually coexist which may cooperatively affect the electron transfer between MOFs and analytes. This will consequently affect the luminescent properties of LMOFs. However, little is known about how these two weak forces collaborate during the luminescent sensing processes of LMOFs. Also, which of them plays a more significant role still remains uncovered.

Herein, we comprehensively studied the explosives detection mechanism of LMOF 1 by theoretically exploring the interactions between 1 and three analytes from three molecule groups (nitroaromatic, benzene hydrocarbon and ketone) with the aid of density functional theory (DFT) and time-dependent density functional theory (TD-DFT). Periodic structures were used to study the adsorption of analytes as well as their effects on the electronic structures of LMOF 1. Cluster models were then employed to further look into the electronic couplings between the analytes and sensor. Through all the above calculations and analyses, we have been able to prove that the luminescent quenching of LMOF 1 in the presence of nitrobenzene is due to the intermolecular electron transfer. A new and major pathway of this intermolecular electron transfer is put forward for the first time which is essentially different from the previously proposed pathway.[16-19,29] Besides, the roles of hydrogen bonding interaction and π-π stacking interaction during the electron transfer processes have been revealed which indicate the two forces

cooperate with each other. To the best of our knowledge, this is the first article concentrating on the cooperative effects of these two weak forces on the luminescent quenching processes of LMOFs. All these findings shed light on the analyte-sensor interactions at the electronic level and would provide useful perspectives into the selection of ligands (at least selection of functional groups of the ligands) in the design of explosives detecting LMOF sensors.

Computational methods

Methods for periodic models

First, we optimized the unit cell structure of LMOF 1. DFT calculations were performed using periodic plane-wave methods with Brillouin-zone sampling restricted to the Γ point. The crystal structure was fully relaxed and lattice parameters were optimized which were in good agreement with the experimental data (see Table S1, Supporting Information). This confirmed the validity of our computational methods. Then, unit cell of LMOF 1 was doubled in the b direction to get the supercell structure before simulating the adsorption of different analytes. Next, this periodic supercell structure and the supercell structures with adsorbed analytes were optimized with respect to all atomic positions considering fixed lattice parameters with Brillouin-zone sampling restricted to the Γ point. Based on the optimized supercell structure with adsorbates, analyte-sensor interaction energies were calculated using the following equations:

$$E_{interaction}=E_{LMOF}+E_{analyte}-E_{LMOF+analyte} \quad (1)$$

For the optimization of the supercell structure with adsorbates as well as the calculation of analyte-sensor interaction energies, dispersion corrections were systematically included within the DFT-D2 method of Grimme[33]. Local density of states (LDOS) projected on the analytes were also obtained based on the optimized structures with the k-point grid of 2×2×1 (this setting was found to be adequate to give preliminary insights into the electronic coupling between analytes and sensor) using the Monkhorst-Pack scheme. All the calculations for the periodic structures were performed using the CASTEP[34] module implemented in the Material Studio 6.0 program suite with a kinetic energy cutoff of 600 eV. The exchange-correlation functional was treated within the generalized gradient approximation (GGA) parametrized by Perdew, Burke, and Ernzernhof (PBE).[35] Ultrasoft pseudo-potentials were applied throughout the computation. A criterion of 5.0e-7 eV/atom was placed on the self-consistent convergence of the total energy. Atomic positions were considered converged until forces were less than 0.01 eV/Å. In order to further test the performance of our theoretical methods, GGA/PW91 functional[36] was also applied in the unit cell optimization with the same basis sets. Besides, DMol3/PBE/DNP[37,38] results for the unit cell optimization were also obtained for comparison.

Methods for cluster models

For the clusters calculations, Gaussian 09 software package[39] was applied to obtain the first one hundred low-lying excitation energies for all the clusters using TD-DFT method. Solvent effects are not included in this article based on the fact that the experiment[22] was carried out in an acetonitrile suspension and LMOF 1 is not soluble (see detailed explanations in Supporting Information below Table S3). Based on the excitation energy, the molecular orbitals involved in the excitation processes were confirmed. Then, analyte-sensor interactions between the framework and analytes were investigated by analyzing the fragment orbitals' contributions for the molecular orbitals involved in the excitation processes. Herein, the fragment orbitals related to the excitation processes were confirmed. Wavefunctions of these fragment orbitals were then generated. These wavefunctions were further multiplied with each other using Multiwfn 3.2.1 program[40,41] to obtain the intermolecular orbital overlap integral values between analytes and the framework. The overlap value can reflect the electronic coupling between the two orbitals and was used in this contribution to visually and quantitatively measure the intermolecular interactions between MOF and nitrobenzene. All the above calculations were performed at the wb97xd/genecp level of theory. Los Alamos National Laboratories 2 Double Zeta basis set and pseudo-potentials (Lanl2dz[42]) were used for zinc atoms while 6-31g(d,p) basis set was taken for other atoms (C, H, N, O). Wb97xd functional[43] is a long-range corrected hybrid functional including empirical dispersion which has given very good performances when dealing with weak intermolecular interactions such as hydrogen bonding and π-π stacking interactions.[44-46] Thus, we have enough confidence that the level of theory used for the clusters calculations is good enough.

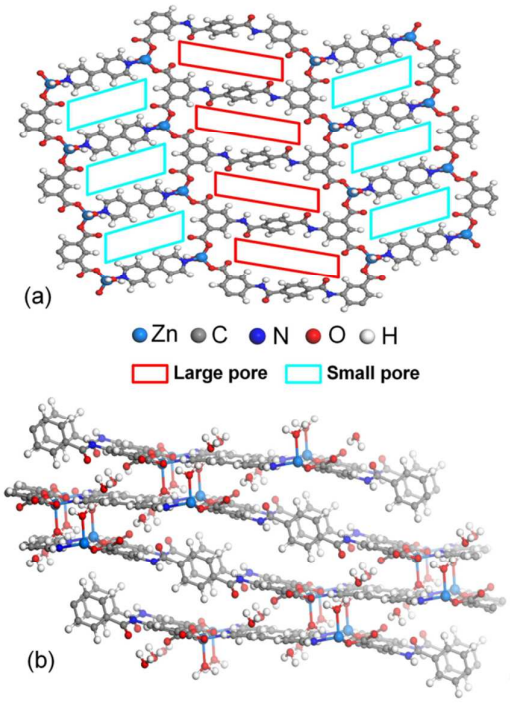

Figure 1. Structural features of LMOF **1**. Top view (a); side view (b).

Results and discussions

A brief description of the LMOF 1 crystal structure

To understand the explosives detecting mechanism and the roles of intermolecular forces, we should first have a deep understanding of the crystal structure especially the potential binding sites inside the MOF. As shown in Figure 1, each Zn (II) ion is four-coordinated by two oxygen atoms from two L^{4-} ligands, one nitrogen atom from a bipy ligand and one oxygen (see detailed information in reference 22) atom from a coordinated water molecule, showing a slightly distorted tetrahedron structure with two kinds of pores. These two pores with different sizes and spatial structures are the most important features of this LMOF which could serve as the sites to encapsulate the analytes and achieve explosives detections. Figure 1 shows that each small pore is formed via two bipy ligands and four Zn (II) ions. The small pore has a length of 10.2 Å and a width of 9.6 Å with two coordinated water molecules penetrating into it, which makes it rather jammed. This indicates its inability to further encapsulate analyte molecules and thus the small pore should stay inactive during the detecting processes. For the large pores, each of them is formed via two L^{4-} ligands together with four Zn (II) ions with a length of 12.8 Å and a width of 9.6 Å (lengths of the two kinds of pores are defined as the distances of the two diagonal carboxylate oxygen atoms, widths are defined as the centroid distances of the two parallel phenyl rings). These pores are quite large and open which provide enough space for the encapsulation of analytes. Thus, the chemical environments of the large pores as well as the analyte-sensor interacting patterns inside them should be investigated.

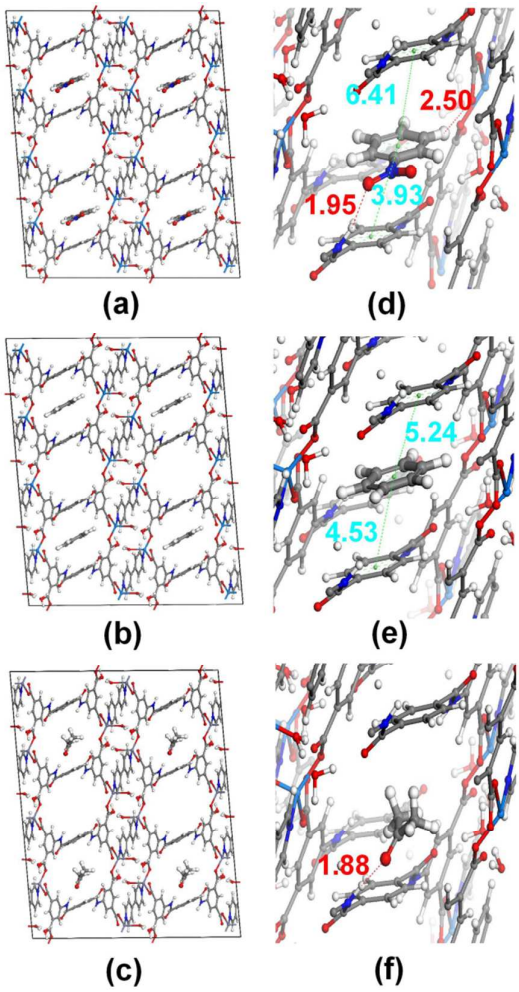

Figure 2. Geometries of LMOF 1 optimized by DFT-D calculations for the adsorption of (a) nitrobenzene, (b) benzene and (c) acetone. Figures d, e, f are magnifications of figures a, b, c respectively. Hydrogen bond lengths are given in red fonts and centroid distances between aromatic rings are given in cyan fonts.

Binding patterns and binding energies analyses

To investigate the analyte-sensor interaction inside the large pores, three analyte molecules namely nitrobenzene, benzene and acetone have been chosen. Consequently we've obtained three optimized supercell structures namely NB-MOF (one nitrobenzene molecule encapsulated into the large pore of LMOF 1), Ben-MOF (one benzene molecule encapsulated into the large pore of LMOF 1), AC-MOF (one acetone molecule encapsulated into the large pore of LMOF 1). Also the supercell structure of LMOF 1 without analyte has been optimized for comparison. For NB-MOF, as shown in Figure 2a and Figure 2d, there is a strong hydrogen bond (1.95 Å) between the nitro group of nitrobenzene and the imino group of the framework. Also, the centroid distance between the aromatic ring of nitrobenzene and that of the framework is quite short (3.93 Å), indicating a pretty strong π-π stacking interaction. It is worth noting that the aromatic imino fragment of the framework has electron donating ability while the nitrobenzene is electron deficient. Thus, these two relatively strong intermolecular forces between the two components may facilitate the electron transfer between them, which leads to the luminescence quenching detection of nitrobenzene. For the case of Ben-MOF (Figure 2b, Figure 2e), the π-π stacking interactions should be much weaker as the distances between the corresponding centroids are much longer (4.53 Å and 5.24 Å respectively). Besides, the lack of hydrogen bonds and the relative electron-rich nature of benzene will also retard the electron transfer. Thus benzene shows neglectable effect on the luminescent properties of the framework which is also supported by experimental results.[22] As for AC-MOF (Figure 2c, Figure 2f), strong hydrogen bond is observed (1.88 Å) between the carbonyl group of acetone and the aromatic imino

group of the framework. The electron deficiency of the carbonyl group as well as the presence of strong hydrogen bond may also provide chances of electron transfer. The experimentally observed absence of luminescence quenching when interacting with acetone may be originated from the lack of π-π stacking interactions.

Table 1. Binding energies for the three analytes.

Structure	Binding energy (eV)
NB-MOF	1.068
Ben-MOF	0.691
AC-MOF	0.852

To give a quantitative view of the intermolecular interaction strengths, we have calculated the binding energies for the three analytes (equation 1) which are reported in Table 1. As is shown, the binding energy of nitrobenzene is somewhat larger than those of other two analytes, which suggests that the coexistence of hydrogen bonding interaction and π-π stacking interaction can enhance the analyte-sensor binding strengths to some extent. This may increase the degrees of electronic coupling and facilitate the intermolecular electron transfer which needs further discussions.

A primary view of the electronic structures

Next, a preliminary view of the electronic couplings between the analytes and sensor is given by calculating the electronic density of states (DOS) as well as local density of states (LDOS) projected onto the adsorbates. As displayed in Figure 3b, the adsorption of nitrobenzene into LMOF 1 causes a clear increase of the main peak value just below the Fermi level. This indicates strong hybridizations of the frontier occupied orbitals of nitrobenzene with VB of LMOF 1. Besides, the encapsulation of nitrobenzene also brings out a new peak just around the bottom of the CB of the framework with an obvious overlapping zone. This suggests the existence of moderate interactions between the unoccupied orbitals of the analyte (nitrobenzene) and CB of the sensor (LMOF 1). Thus, we can get that, the electronic structure of LMOF 1 is quite sensitive for the presence of nitrobenzene. The considerable hybridizations of molecular orbitals and bands between nitrobenzene and LMOF 1 increase chances of intermolecular electron transfer which consequently induce luminescence quenching. When comes to the case of Ben-MOF, the above interactions are quite different. The VB has overlaps with the occupied orbitals of benzene closer to the VB top, indicating strong electron donating ability of benzene. In this case, electrons may prefer to transfer from benzene to MOF. Besides, the adsorption of benzene does not bring apparent changes to the CB of the framework. Thus, electron transfer from CB to LUMO of benzene is undesirable. Benzene cannot accept electrons from the framework. As for AC-MOF, the encapsulation of acetate bring little changes to the DOS right below the Femi level but, indeed, changes the DOS well above it. As plotted in Figure 3d, there is a clear overlap in the region 3.0-4.0 eV. This demonstrates strong interactions between the unoccupied orbitals of acetone and CB of the framework. However, compared to the case of NB-MOF, this overlap locates in the high energy zone which is not involved in the photo-excitation process. Thus, this overlap will not affect the luminescent properties of LMOF 1, making the framework inert to acetone.

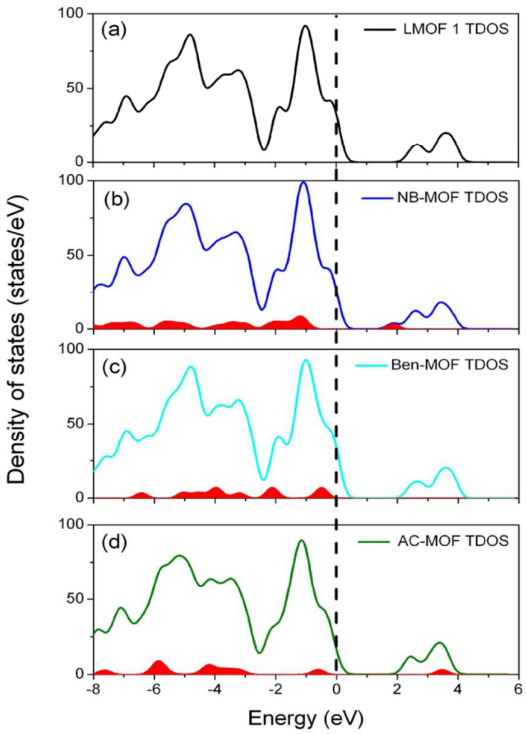

Figure 3. The total electronic DOS (TDOS) for (a) LMOF 1, (b) NB-MOF, (c) Ben-MOF and (d) AC-MOF. The local DOS projected onto the analytes are also plotted (red filled areas under DOS curves). The Fermi level is indicated by the vertical dashed lines.

As discussed above, by investigating the analyte-sensor interactions from the view of binding patterns to inherent electronic structures, we have get a deep understanding of the roles of analyte-sensor interactions in the explosives detection processes of LMOF 1. The strong electronic coupling between the analyte and the framework near the Fermi level is found to be a prerequisite for electron transfer. Intermolecular hydrogen bond and π-π stacking seem to facilitate this coupling and play unknown roles. To get a detailed picture on how these two weak forces function and which of them plays a more significant role during the electron transfer process we take a further step into the electronic properties of the four above mentioned structures (LMOF 1, NB-MOF, Ben-MOF, AC-MOF). The possible intermolecular electron transfer pathways are also investigated. In the sections below, cluster models of the four structures have been applied to study these issues.

Descriptions of the cluster models

Truncated cluster models from the periodic crystal structures have been successfully applied in studies of the electronic properties of metal organic frameworks.[47-53] In this paper, four clusters namely CL-LMOF 1, CL-NB-MOF, CL-Ben-MOF and CL-AC-MOF are obtained by truncating from the corresponding optimized periodic structures. H atom is used to balance the overall charges such that the truncated structures remained neutral. Because we are using finite clusters to represent periodic structures for the study of analyte-sensor interactions, these structures should be delicately selected to best represent the local environment of the corresponding analyte. Also by taking computational costs into consideration, we choose four clusters each has approximately 130 atoms (shown in Figure S2, Supporting Information).

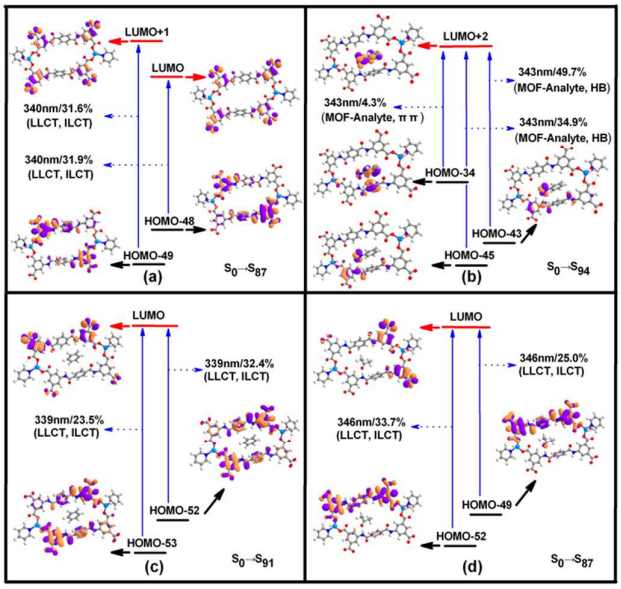

Figure 4. Molecular orbitals involved in the excitation processes for (a) LMOF 1, (b) CL-NB-MOF, (c) CL-Ben-MOF and (d) CL-AC-MOF. Corresponding excitation wavelengths, transition contributions (given in percentage) and excitation features are also given in this picture. LLCT represents ligand to ligand charge transfer, ILCT represents intra-ligand charge transfer, "MOF-Analyte HB" represents electron transfer from MOF to analyte molecule via hydrogen bond and "MOF-Analyte π π" represents electron transfer from MOF to analyte molecule via π-π stacking. All the contour thresholds for the molecular orbitals are plotted with the contour value set to 0.02.

Excitation processes and flows of electrons

Excitations of LMOFs from ground states to electronic excited states frequently trigger inter and intra molecular electron transfer. A good understanding of the excitation process will provide useful insights into the flow of electrons upon photo-excitation. Thus, the first one hundred low-lying excited state energies of the four clusters have been obtained by TD-DFT calculations to primarily study the excitation processes. Based on the fact that the emission spectra are obtained by exciting the samples at the 350 nm absorption peak,[22] we have carefully studied the electronic transition states and features corresponding to this excitation. As reported in Table S3 (Supporting Information), the excitation of LMOF 1 at 350 nm in the experiment corresponds to the $S_0 \rightarrow S_{87}$ (calculated value 340 nm) electronic transition of the corresponding cluster model. Figure 4a shows the corresponding molecular orbitals involved in this transition. As plotted in this picture, the transition shows a ligand to ligand charge transfer (LLCT) feature as well as an intra-ligand charge transfer (ILCT) feature, indicating the luminescence of LMOF 1 is linker based. For the case of CL-NB-MOF, the electronic transitions corresponding to the 350 nm excitation are also reported. Essentially different from the former case, the excitation at 350 nm corresponds to a $S_0 \rightarrow S_{94}$ (calculated value 343 nm) transition which features significant intermolecular electron transfer from the framework to nitrobenzene. As plotted in Figure 4b, the main compositions (84.6% in total) for this transition are HOMO-45→LUMO+2 and HOMO-43→LUMO+2. The occupied orbitals (H-45 and H-43) locate considerably on the imino group of the framework and the nitro group of the analyte, which is linked by a strong hydrogen bond. Whereas, the LUMO+2 orbit locates dominantly on the analyte. This indicates that the hydrogen bond between these two groups should facilitate the intermolecular electron transfer process. Besides, there is also a small composition (4.3%) corresponding to HOMO-34→LUMO+2. In this case, the occupied orbit (H-34) mainly locates on the two proximate aromatic rings of the analyte and the framework which suggests that π-π stacking interaction may also take part in the electron transfer process. One should notice that the $S_0 \rightarrow S_{93}$ transition and $S_0 \rightarrow S_{95}$ transition also contribute to the excitation of NB-MOF around 350 nm, both of which show ligand to ligand charge transfer (LLCT) features. These contributions are rather small and corresponding orbitals are located within the framework, leaving nitrobenzene unexcited. For the other two clusters (CL-Ben-MOF and CL-AC-MOF), the excitation processes are much like the case of CL-LMOF 1 which means that the two analytes (benzene and acetone) scarcely participate in the excitation processes (this is further confirmed via fragment orbital interaction analyses which are shown in Figure S4 and Figure S5,

Supporting Information). To sum up, the above analyses provide direct evidence of the presence of intermolecular electron transfer in the case of CL-NB-MOF as well as the absence of it in other two cases. This further denotes that the luminescence quenching of LMOF 1 with nitrobenzene is through a donor-acceptor electron transfer mechanism. Considering the fact that H-45 and H-43 orbitals (favor hydrogen bond interaction) have much larger compositions than that of H-34 orbit (favors π-π stacking interaction), hydrogen bonding interaction seems to play a more significant role than π-π stacking interaction during this electron transfer process. However, this issue should be further investigated.

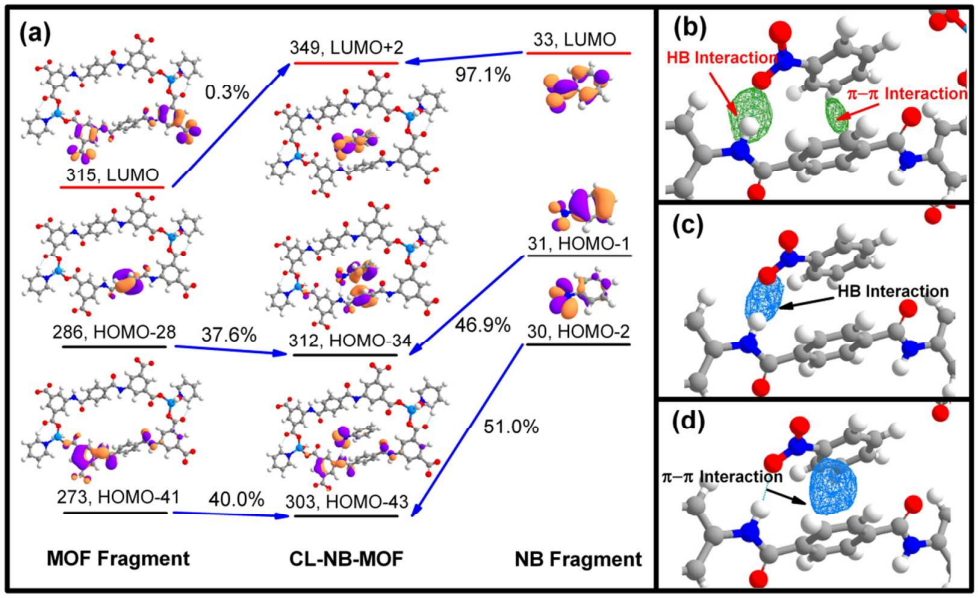

Figure 5. (a) Fragment orbital interaction diagram for CL-NB-MOF with contour value set to 0.02 (for clarity, only orbitals related to the $S_0 \rightarrow S_{94}$ excitation process are plotted). Intermolecular orbital overlap zone between (b) 315 orbit of fragment MOF and 33 orbit of fragment NB (contour value=0.00001), (c) 273 orbit of fragment MOF and 30 orbit of fragment NB (contour value=0.0001), (d) 286 orbit of fragment MOF and 31 orbit of fragment NB (contour value=0.0003). The green surfaces represent the overlap zones between unoccupied fragment orbitals and the blue surfaces represent the overlap zones between occupied fragment orbitals. The interaction type is also given. Different contour values are chosen to best visualize all the interactions while unanimous contour value, which is not applied, will lead to messy graphs.

Fragment orbital interactions and intermolecular orbital overlaps

Herein, we take a further step to investigate the aforementioned two interactions as well as the potential electron transfer pathways from the view of fragment orbitals. The CL-NB-MOF structure is divided into two fragments namely the MOF fragment and the NB (nitrobenzene) fragment. Firstly, we obtained the fragment orbital interaction diagram (see detailed information in Figure S3, Supporting Information) between the two fragments. Compositions of the molecular orbitals related to the $S_0 \rightarrow S_{94}$ electronic transition (orbital number 301, 303, 312, 349) are analyzed. Then, the corresponding fragment orbitals and complex orbitals are plotted in Figure 5a (as the compositions of complex orbit HOMO-45 are very similar to those of HOMO-43, this orbit is not discussed in this article).

As shown in this picture, for the unoccupied complex orbit 349, the 315 orbit from MOF fragment contributes merely 0.3% while the 33 orbit from NB fragment contributes as much as 97.1%. Then, we obtained the intermolecular orbital overlap integral between 315 and 33 by multiplying the wavefunctions of the two fragment orbitals. The value of the overlap integral is only 0.0006 and the overlap zone is plotted in Figure 5b. As clearly shown in this picture, the overlap zone locates at both the hydrogen bonding zone and the middle of the aromatic rings which directly proved that hydrogen bond and π-π stacking all facilitate the intermolecular electron transfer process. However, as stated above, the fragment orbital interactions and intermolecular orbital overlaps for the two empty fragment orbitals are very weak. Also, the energy gap between the two orbitals (315 has much lower energy than that of 33, see details in Figure S3, Supporting Information) does not favor the electron transfer from MOF to nitrobenzene (notice that although 317 orbital energy of MOF is close to that of 33, this orbit does not participate in the excitation process. Figure S3, Supporting Information). All these phenomena seem to reveal that the intermolecular electron transfer upon excitation cannot happen from the LUMO of MOF to LUMO of

nitrobenzene. However, one should always keep in mind that these calculations are performed using a cluster model. The authentic periodic structure will broaden the LUMO orbit of MOF cluster into a wide unoccupied band (known as conduction band), which makes the electronic coupling between the unoccupied orbitals of the analyte and sensor stronger. Thus, we can infer that the electron transfer from the VB of MOF to CB of MOF then to LUMO of nitrobenzene will be a possible but nonessential pathway (Figure 6a). Intermolecular transfer via this pathway is facilitated by both hydrogen bond and π-π stacking.

For the case of complex orbitals HOMO-34 and HOMO-43, both the occupied orbitals are largely composed from the two fragment orbitals. This indicates strong electronic coupling between MOF and nitrobenzene through occupied fragment orbitals. For complex orbit 303, the 273 orbit from MOF fragment contributes 40.0% while the 30 orbit from nitrobenzene contributes 51.0%. As shown in Figure 5a, the 273 orbit locates significantly on the imino group while the 30 orbit locates mainly on the nitro group. This reveals that the interactions between the two orbitals are mainly facilitated by hydrogen bond. Then, the intermolecular orbital overlap integral between 273 and 30 is obtained. The value of the overlap integral is 0.0045 and the overlap zone is plotted in Figure 5c. As shown in this picture, the overlap zone locates along the hydrogen bond which directly proves that hydrogen bond serves as the bridge for intermolecular electron transfer. When comes to complex orbit 312, the 286 orbit from MOF fragment contributes 37.6% while the 31 orbit from nitrobenzene contributes 46.9%. Different from the former case, both the 286 orbit and the 31 orbit locate mainly on the aromatic ring of MOF and nitrobenzene, respectively. This suggests that the interactions between the two orbitals are mainly facilitated by π-π stacking. The intermolecular orbital overlap zone between 286 and 31 are also plotted with a value of 0.0184. As shown in Figure 5d, this overlap zone mainly locates between the two aromatic rings which is obviously of π-π feature. The value of this overlap is much larger than the former one which indicates that the π-π interaction is more efficient for electron transfer between the two components.

For CL-Ben-MOF and CL-AC-MOF, the molecular orbitals involved in the excitation (282, 283, 336 for CL-Ben-MOF and 278, 281, 331 for CL-AC-MOF) are solely based on the MOF fragment (Figure S4, Figure S5, Supporting Information) which means the interactions between the framework and the corresponding analytes are very weak. Thus, intermolecular orbital overlap analyses in these two cases are not performed.

All in all, the large fragment orbital interactions and intermolecular orbital overlaps between the occupied orbitals of MOF and nitrobenzene indicate a strong electronic coupling between nitrobenzene and the framework via occupied fragment orbitals. The small fragment orbital interactions and intermolecular orbital overlaps between the LUMO of MOF and the LUMO of nitrobenzene indicate a weak electronic coupling between nitrobenzene and the framework via unoccupied fragment orbitals. Thus, the electrons in the VB of LMOF 1 can be directly photo-excited to the LUMO of nitrobenzene which should be the major pathway for the intermolecular electron transfer processes (Figure 6a). Hydrogen bonding interaction is less efficient in electron transfer (low overlap value) but possesses large composition in the electron transfer process (84.6%) while the π-π stacking interaction is more efficient in electron transfer (much larger overlap value) but with much smaller composition (4.3%). Thus, we can conclude that, in the interaction of LMOF 1 with nitrobenzene, hydrogen bond and π-π stacking play comparable roles in the transfer of electrons (Figure 6b).

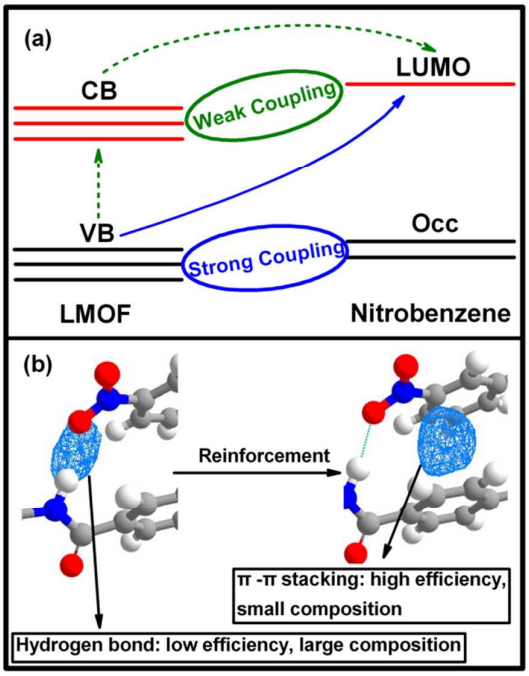

Figure 6. (a) Two pathways for intermolecular electron transfer. Green dashed arrows represent the nonessential pathway. Blue solid arrow represents the essential pathway. Occ represents the occupied orbitals of nitrobenzene concerned in the analyte-sensor interactions. (b) Schematic diagram showing the roles of hydrogen bond, π-π stacking as well as their cooperative effects in processes of intermolecular electron transfer.

Cooperation of hydrogen bond and π-π stacking

From the combined information on the above two sections we come to realize that both the two interactions play important roles. π-π stacking interactions, which provide considerable orbital overlaps, show higher efficiency for electron transfer due to the delocalized π-electrons on the aromatic rings.[32] However, as revealed by previous works, π-π stacking interactions are usually quite weak due to Coulombic repulsions between adjacent rings.[54-56] This makes the approaching of two rings hard which could not provide adequate overlaps for electron transfer. In the case of LMOF 1, the presence of strong hydrogen bond neutralizes the Coulombic repulsion, pull the two rings closer and consequently reinforces the π-π stacking interaction (as directly revealed by the large binding energy and short centroids distance between nitrobenzene and LMOF 1). Thus, the hydrogen bond not only serves as the electron transfer bridge but more importantly, cooperates with the π-π stacking which induces strong luminescence quenching. This kind of cooperation inside the LMOF sensor is investigated for the first time in this contribution which is highly possible to exist in many other similar cases.

Conclusions

In summary, we have theoretically investigated the analyte-sensor interactions between LMOF 1 and three analyte molecules from different molecular groups. The luminescence quenching of LMOF 1 when interacting with nitrobenzene is proved to be the intermolecular electron transfer from the framework to the analyte. We have proposed, for the first time, that the electronic coupling between the framework and nitrobenzene is so strong that the electrons in the VB of LMOF 1 can be directly photo-excited to the LUMO of nitrobenzene which is essentially different from the previous mechanism. Meanwhile, we have also discovered that the absences of intermolecular electron transfer in the other two cases are responsible for the absences of luminescence quenching. As revealed in this paper, both hydrogen bond and π-π stacking serve as bridges for the intermolecular electron transfer and play comparable roles. π-π stacking is found to be a more efficient channel for electron transfer while hydrogen bond reinforces the π-π stacking interaction. The cooperation of the two interactions can lead to significant luminescence quenching of LMOF in the presence of nitrobenzene. Thus we can expect that, for the luminescence quenching detection of nitroaromatics, a considerable π-π stacking interaction between the analyte and

sensor should be essential. The MOF ligands should chiefly contain accessible aromatic rings. Besides, by introducing hydrogen and electron donating functional groups (such as amino and imino) into proper sites adjacent to the aromatic ring, the analyte-sensor interaction can be further strengthened by intermolecular hydrogen bond. This will "activate" the high efficiency (π-π) electron transfer channel and consequently lead to high sensitive luminescence quenching.

Acknowledgements

This work is supported by the National Natural Science Foundation of China (Grant Nos. 21137001, 21036006, 21373042).

Notes and references

[a] State Key Laboratory of Fine Chemicals, Dalian University of Technology, Dalian 116024, China. haoce@dlut.edu.cn

[b] State Key Laboratory of Molecular Reaction Dynamics, Dalian Institute of Chemical Physics, Chinese Academy of Sciences, Dalian 116023, China.

The authors declare no competing financial interest.

Electronic Supplementary Information (ESI) available: [Figure S1 shows the structure of the organic ligand; Figure S2 shows the structures of the cluster models; Figure S3, S4 and S5 show the detailed information of the fragment orbital interactions between the framework and analytes; Table S1 shows the calculated crystal lattice parameters as well as the corresponding experimental data; Table S2 gives the binding energies for the adsorbates in detail. Table S3 reports the calculated excitation energies for the aforementioned four clusters. Table S4 reports the calculated excitation energies with and without solvation effects for CL-MOF 1.].

1 K. G. Furton and L. J. Myers, *Talanta.*, 2001, 54, 487–500.

2 G. A. Eiceman and J. A. Stone, *Anal. Chem.*, 2004, 76, 390–397.

3 J. M. Sylvia, J. A. Janni, J. D. Klein and K. M. Spencer, *Anal. Chem.*, 2000, 72, 5834–5840.

4 R. D. Luggar, M. J. Farquharson, J. A. Horrocks and R. J. Lacey, *X-Ray Spectrom.*, 1998, 27, 87–94.

5 M. E. Germain and M. J. Knapp, *Chem. Soc. Rev*., 2009, 38, 2543–2555.

6 S. W. Thomas, G. D. Joly and T. M. Swager, *Chem. Rev*., **2007**, *107*, 1339–1386.

7 D. Gopalakrishnan and W. R. Dichtel, *J. Am. Chem. Soc*., 2013, 135, 8357–8362.

8 B. Gole, S. Shanmugaraju, A. K. Bar and P. S. Mukherjee, *Chem. Commun.*, 2011, 47, 10046–10048.

9 M. D. Allendorf, C. A. Bauer, R. K. Bhakta and R. J. T. Houk, *Chem. Soc. Rev.*, 2009, 38, 1330–1352.

10 B. L. Chen, S. Xiang and G. Qian, *Acc. Chem. Res.*, 2010, 43, 1115–1124.

11 L. E. Kreno, K. Leong, O. K. Farha, M. Allendorf, D. R. P. Van and J. T. Hupp, *Chem. Rev.*, 2012, 112, 1105–1125.

12 B. Liu *J. Mater. Chem.*, 2012, 22, 10094–10101.

13 Y. Cui, Y. Yue, G. Qian and B.L. Chen, *Chem. Rev*., 2012, 112, 1126–1162.

14 Z. C. Hu, B. J. Deibert and J. Li, *Chem. Soc. Rev*., 2014, 43, 5815–5840.

15 D. Banerjee, Z. C. Hu and J. Li, *Dalton Trans.*, 2014, 43, 10668–10685.

16 S. C. Pramanik, X. Zheng, T. Zhang, J. Emge and J. Li, *J. Am. Chem. Soc.*, 2011, 133, 4153–4155.

17 D. Banerjee, Z. Hu, S. Pramanik, X. Zhang, H. Wang and Li, J. *CrystEngComm*, 2013, 15, 9745–9750.

18 B. Gole, A. K. Bar and P. S. Mukherjee, *Chem. Eur. J.*, 2014, 20, 2276–2291.

19 G. L. Liu, Y. J. Qin, J. Li, G. Y. Wei and H. Li, *Chem. Commun.*, 2013, 49, 1699–1701.

20 A. Lan, K. Li, H. Wu, D. H. Olson, T. J. Emge, W. Ki, M. Hong and J. Li, *Angew. Chem. Int. Ed.*, 2009, 48, 2334–2338.

21 A. Lan, K. Li, H. Wu, L. Kong, N. Nijem, D. H. Olson, T. J. Emge, Y. J. Chabal, D. C. Langreth, M. Hong and J. Li, *Inorg. Chem.*, 2009, 48, 7165–7173.

22 G. Y. Wang, L. L. Yang, Yue. Li, Han. Song, W. J. Ruan, Ze. Chang and X. H. Bu, *Dalton Trans.*, 2013, 42, 12865–12868.

23 D. X. Ma, B. Y. Li, X. J. Zhou, Q. Zhou, K. Liu, G. Zeng, G. H. Li, Z. Shi and S. H. Feng, *Chem. Commun.*, 2013, 49, 8964–8966.

24 G. Y. Wang, C. Song, D. M. Kong, W. J. Ruan, Ze. Chang and Yue. Li, *J. Mater. Chem. A*, 2014, 2, 2213–2220.

25 Z. Feng, W. B. Tan, M. L. Feng, A. J. Lana and X. Y. Huang, *J. Mater. Chem. A*, 2014, 2, 6426–6431.

26 B. L. Chen, S. Ma, F. Zapata, E. B. Lobkovsky and J. Yang, *Inorg. Chem.*, 2006, 45, 5718–5720.

27 T. K. Kim, J. H. Lee, D. Moon and H. R. Moon, *Inorg. Chem.*, 2013, 52, 589–595.

28 Z. Hu, S. Pramanik, K. Tan, C. Zheng, W. Liu, X. Zhang, Y. J. Chabal and J. Li, *Cryst. Growth Des.*, 2013, 13, 4204–4207.

29 S. Pramanik, Z. Hu, X. Zhang, C. Zheng, S. Kelly and J. Li, *Chem. Eur. J.*, 2013, 19, 15964–15971.

30 G. J. Zhao and K. L. Han, *Acc. Chem. Res.*, 2012, 45, 404–413.

31 K. L. Han and G. J. Zhao, *Hydrogen Bonding and Transfer in the Excited State*, John Wiley & Sons Ltd.: Chichester, U.K., 2011, Vol. I & II.

32 D. B. Hall, R. E. Holmlin and J. K. Barton, *Nature.*, 1996, 382, 731–735.

33 S. Grimme, *J. Comput. Chem.*, 2006, 27, 1787–1799.

34 S. J. Clark, M. D. Segall, C. J. Pickard, P. J. Hasnip, M. J. Probert, K. Refson and M. C. Z. Payne, *Z. Kristallogr.*, 2005, 220, 567–570.

35 J. Perdew, K. Burke and M. Ernzerhof, *Phys. Rev. Lett.*, 1996, 77, 3865.

36 J. P. Perdew, J. A. Chevary, S. H. Vosko, K. A. Jackson, M. R. Pederson, D. J. Singh and C. Fiolhais, *Phys. Rev. B*, 1992, 46, 6671–6687.

37 B. Delley, *J. Chem. Phys*., 1990, 92, 508–517.

38 B. Delley, *J. Chem. Phys*., 2000, 113, 7756–7764.

39 M. J. Frisch, G. W. Trucks, H. B. Schlegel, G. E. Scuseria, M. A. Robb, J. R. Cheeseman, G. Scalmani, V. Barone, B. Mennucci, G. A. Petersson, et al., *Gaussian 09*, revision C.01; Gaussian, Inc.: Wallingford, CT, 2009.

40 T. Lu and F. W. Chen, *J. Comput. Chem.*, 2012, 33, 580–592.

41 T. Lu and F. W. Chen, *J. Mol. Graphics Modell.*, 2012, 38, 314–323.

42 P. J. Hay and W. R. Wadt, *J. Chem. Phys*., 1985, 82, 299–310.

43 J. Chai and M. H. Gordon, *J. Chem. Phys*., 2008, 128, 084106.

44 Peng. Gu, R. Q. Lu, D. Liu, Y. K. Lu and S. T. Wang, *Phys. Chem. Chem. Phys*., 2014, 16, 10531–10538.

45 T. B. Tai and M. T. Nguyen, *Chem. Commun.*, 2013, 49, 913–915.

46 S. Panigrahi, A. Bhattacharya, S. Banerjee and D. Bhattacharyya, *J. Phys. Chem. C*, 2012, 116, 4374−4379.

47 L. Grajciar, A. D. Wiersum, P. L. Llewellyn, J. S. Chang and P. Nachtigall, *J. Phys. Chem. C*, 2011, 115, 17925–17933.

48 A. L. Dzubakl, L. C. Lin, J. H. Kim, J. A. Swisher, R. Poloni, S. N. Maximoff, B. Smit and L. Gagliardi, *Nat. Chem.*, 2012, 4, 810–816.

49 M. Ji, X. Lan, Z. P. Han, C. Hao and J. S. Qiu, *Inorg. Chem.*, 2012, 51, 12389–12394.

50 X. Sui, M. Ji, X. Lan, W. H. Mi, C. Hao and J. S. Qiu, *Inorg. Chem.*, 2013, 52, 5742–5748.

51 M. Ji, C. Hao, D. D. Wang, H. Li and J. S. Qiu, *Dalton Trans.*, 2013, 42, 3464–3470.

52 M. X. Zhang, W. H. Mi and C. Hao, *Commun. Comput. Chem.*, 2013, 1, 269–281.

53 S. H. Kang, Z. Q. Liu, J. J. Tan, C. Hao and J. S. Qiu, *Commun. Comput. Chem.*, 2014, 2, 69–87.

54 C. A. Hunter and J. K. M. Sanders, *J. Am. Chem. Soc.*, 1990, 112, 5525–5534.

55 F. Cozzi, J. M. Cinquini, R. Annunziata, T. Dwyer and J. S. Siegel, *J. Am. Chem. Soc.*, 1992, 114, 5729–5733.

56 F. Cozzi, J. M. Cinquini, R. Annunziata and J. S. Siegel, *J. Am. Chem. Soc.*, 1993, 115, 5330–5331.

Graphical abstract

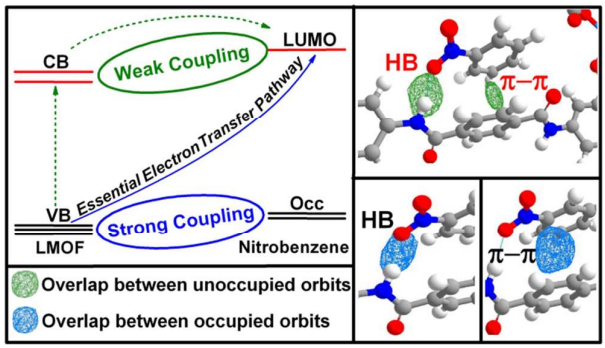

For the first time, hydrogen bond and π–π stacking are demonstrated to play cooperative roles in the intermolecular electron transfer process from nitrobenzene to MOF sensor, which lead to the luminescence quenching detection of nitrobenzene.